Available online at www.sciencedirect.com

ScienceDirect

Publishing Services by Elsevier

International Journal of Naval Architecture and Ocean Engineering 9 (2017) 705–719

http://www.journals.elsevier.com/international-journal-of-naval-architecture-and-ocean-engineering/

A new procedure for load-shortening and -elongation data for progressive collapse method

Jonathan Downes [a], Gökhan Tansel Tayyar [b], Illia Kvan [c], Joonmo Choung [c,*]

[a] Fluid Structure Interactions Group, Faculty of Engineering and the Environment, University of Southampton, Southampton, SO16 7QF, UK
[b] Department of Naval Architecture and Marine Engineering, Istanbul Technical University, Istanbul, Turkey
[c] Department of Naval Architecture and Ocean Engineering, Inha University, Inha-ro 100, Nam-gu, Incheon, 402-751, Republic of Korea

Received 27 July 2016; revised 13 September 2016; accepted 19 October 2016
Available online 28 December 2016

Abstract

Progressive Collapse Method (PCM) has been broadly applied to predict moment-carrying capacity of a hull girder, however accuracy of PCM has not been much studied. Accuracy of PCM is known to be dependent on how Load-Shortening and -Elongation (LSE) curve of a structural units are well predicted. This paper presents a new procedure to determine LSE datum based on box girder Finite Element Analyses (FEAs) instead of using finite element model of stiffened panels. To verify reliability of FEA results, the simple box girder collapse test results are compared with FEA results of same box girders. It reveals one frame-based box girder model is sufficiently accurate in terms of ultimate strengths of the box girders. After extracting LSE data from the box girders, PCM-based moment-carrying capacities are compared with those from FEAs of the box girders. PCM results are found to be equivalent to FEAs in terms of moment-carrying capacity if accurate LSE data are secured. The new procedure is applied to well-known 1/3 scaled frigate full section. Very excellent moment-carrying capacity of frigate hull section is obtained from PCM with LSE data from box girder FEAs.

Keywords: Progressive collapse method; Load-shortening and elongation data; Box girder; Moment-carrying capacity; Hull girder ultimate strength

1. Introduction

The recent cracking of an 8000 Twenty Equivalent Unit (TEU) sized container carrier reminds us that accurate prediction of moment-carrying capacity of a ship hull girder is of much importance whether it is in intact or damaged condition (NKK, 2014). The accident provides a key motivation that more rigorous approach is necessary to estimate moment-carrying capacities in real ship hull girders.

Caldwell (1965) proposed a simplified formula to predict ultimate strength of an intact hull section and later improvements has been suggested by various authors including Paik and Mansour (1995), Paik et al. (2013), Benson et al. (2013), etc. Recently, many of studies have been toward semi-numerical approaches such as Progressive Collapse Method (PCM) and Idealized Structural Unit Method (ISUM) or pure-numerical approach such as nonlinear Finite Element Analysis (FEA) because they are believed to be more reliable than simplified formulas. Also intelligent supersize finite element method, so called ISFEM, was introduced in a reference (Hughes and Paik, 2010) where hull section is discretized into intelligent supersize plate elements and intelligent supersize beam-column elements. It is known that ISFEM is based on framework of nonlinear FEM but the elements include nonlinear structural behavior so ISFEM does not need to build initial imperfections in modeling stage.

It is believed that nonlinear FEA yields accurate relation of moment-carrying capacity versus curvature increase realizing smooth neutral axis mobility, as long as a sufficient number of finite elements are used. Thus nonlinear FEA can be regarded

* Corresponding author.
E-mail address: jmchoung@inha.ac.kr (J. Choung).
Peer review under responsibility of Society of Naval Architects of Korea.

http://dx.doi.org/10.1016/j.ijnaoe.2016.10.005

Nomenclature

a	Frame spacing
b	Spacing of longitudinal stiffeners
C_p	Initial distortion coefficient in plate
C_s	Initial distortion coefficient in plate-web intersection line
C_w	Initial distortion coefficient in stiffener web
E	Elastic modulus of steel
f_x	Axial force acting on a structural unit
m	Number of half waves in longitudinal direction of plate
n	Number of half waves in transverse direction of plate
R_x, R_x, R_z	Three components for rotational constraint
t	Thickness of steel
t_p	Thickness of plate
T_x, T_y, T_z	Three components for translational constraint
x, y, z	Notations of Cartesian coordinate system
β	Slenderness ratio of plate
δ_p	Magnitude of initial distortion in plate
δ_w	Magnitude of initial distortion in web
ε	Nominal axial strain
ε_{y0}	Yield strain corresponding to initial yield strength
η_p	Breadth of yield stress zone in plate
η_w	Breadth of yield stress zone in stiffener web
ν	Poisson ratio
σ	Axial nominal stress
σ_{y0}	Initial yield strength of steel
σ_{y0p}	Initial yield strength of plate
σ_{y0w}	Initial yield strength of stiffener web
σ_r	Residual compressive stress due to welding
σ_x	Axial stress

as one of the most reliable numerical approaches. Many nonlinear FEA-based publications have been proposed by Amlashi and Moan (2008), Paik et al. (2008), Qi et al. (2005), Xu et al. (2013), etc. However, modeling of initial distortions induced by welding fabrication process is potentially time-consuming. Considering that ultimate and post-ultimate strengths of a hull section are highly susceptible to even slight changes in mode shapes and distortion amplitudes, more efficient approaches can be necessary as a better alternative.

The ISUM provides a more efficient way to reach moment-carrying capacity of a hull girder than FEA, because an elastic and inelastic resistances under each component of external load need to be assigned to an idealized structural unit. These structural resistances can be determined from simple tensile tests, elastic or plastic collapse experiments, or even nonlinear FEA results. For this reason, the structural resistances are capable of inherently incorporating effects of initial imperfections (Paik et al., 1996). Wang et al. (2002) presented hull girder residual strengths using ISUM for various ship types: single and double hull oil tankers and bulk carriers.

PCM was first proposed by Smith (1977). PCM has been widely used to predict moment-carrying capacity of an intact ship section (Gordo and Guedes Soares, 1996, 1997; Gordo et al., 1996; Tayyar et al., 2014; IACS, 2015). Recently, employment of PCM has been extended to asymmetrically damaged hull sections by hiring another convergence criterion which was for determining rotational shift history of hull girder neutral axis (Choung et al., 2012) and to consider a larger compartment based section of the hull girder by Benson et al. (2013).

Even though many studies based on PCM have been proposed, most have shown just comparison of the results based on PCM with those on nonlinear FEAs or experiments. It means more fundamental studies have not been sufficiently shown to improve accuracy of results based on PCM.

There are many other approaches to produce load-shortening data. Multi-bay FE models such as one and two half frame space model, three frame model, even four frame model have been popularly employed. But it is impossible to accurately predict load-shortening data from Multi-bay FE model, because it is already separated from a hull girder and continuous boundary conditions are applied to separated edges. It means that boundary conditions may affect the shortening behavior. After separation of a stiffened panel, it is impossible to consider shear lag effect on a separated stiffened panel. It also means two stiffened panels for which scantlings are same and spatial locations are different always should have same Load-Shortening and -Elongation (LSE) data. But in reality it is not always true. The other alternative to obtain LSE data is empirical formulas. Recently well-proven formulas to predict load-shortening data are presented in H-CSR (IACS, 2015). But they are not able to consider external or internal pressure effect, in addition the load-shortening data from the formulas are much different even from multi-bay FEA results (Nam et al., 2014; Tayyar et al., 2014). Other challenge such as kinematic displacement theory has been also proposed (Tayyar et al., 2014), but it also includes many mechanical assumptions. These disadvantages of the existing approaches become primary motivation of this paper to develop a new procedure from box girder.

This study aims to evaluate relative accuracy of PCM-based result compared to that of nonlinear FEA-based results in terms of first load-shortening and -elongation curves and moment-carrying capacities. Hence this study starts under assumption that PCM is identical with nonlinear FEA as long as exact LSE data are secured. As a first step for verification of the assumption, nonlinear FEAs are to be conducted for the box girders for which a series of collapse tests had been performed by Nishihara (1984). Provided that the FEA results are successfully comparable with test ones, it is thought that nonlinear FEA parameters such as box girder spans, initial imperfection levels, and load/boundary conditions are also verified.

As well known, accuracy of PCM is mostly dependent on accuracy of LSE data. Thus second step is to introduce a new procedure to extract LSE data from the box girder FEA results. Once extracted LSE data are to be used for input data of

UMADS (Choung et al., 2014) which is PCM-based in-house code and capable to import external LSE data to calculate moment-carrying capacities of the box girders. If the moment-carrying capacities are proved to be equivalent to results from nonlinear FEA, then it can be stated that accuracy of PCM is verified.

In discussion, how the new procedure to take LSE data from box girder FEAs out is applied to hull section in reality. Validity of the new procedure to secure LSE curves is provided for 1/3 scale-down frigate test model which was published by Dow (1991).

2. Verification of nonlinear FEA parameters (step I)

2.1. Objective box girders

Nishihara (1984) carried out a series of box girder collapse tests. He took into account four different types of the hull section specimens: MST for single hull tanker, MSD for double bottom tanker, MSB for double bottom bulker, and MSC for double bottom container ship. Base plates with two different thicknesses were used for fabrication of each type of the specimen as shown in Table 1.

It can be considered that test-related uncertainties increase as complex as specimen fabrication process is. For efficient comparative study, the simplest specimens, namely MST-3 and MST-4 box girders in Fig. 1(a), are focused on in this paper. Fig. 1 is the reproduced test schematics from original article for better visibility. As depicted in Fig. 1(b), pure bending moment was applied to the box girders using four point bending apparatus.

2.2. Finite element modeling

Smith et al. (1988) proposed three levels of welding residual stresses as shown in Eq. (1). In this paper, average and severe levels are separately applied to finite element models. Weld-induced yield stress zones can be determined using Eqs. (2) and (3) for base plate and stiffener web, respectively.

$$\sigma_r = \begin{cases} 0.05\sigma_{y0}\ for\ slight \\ 0.15\sigma_{y0}\ for\ average \\ 0.30\sigma_{y0}\ for\ severe \end{cases} \tag{1}$$

$$\eta_p = \frac{\sigma_r}{\sigma_{y0p} + \sigma_r}\frac{b}{2} \tag{2}$$

$$\eta_w = \frac{\sigma_r}{\sigma_{y0w} + \sigma_r} \tag{3}$$

Table 1
Mechanical properties of box girder specimens (Nishihara, 1984).

t (mm)	σ_{y0} (MPa)	E (MPa)	v	Specimen label
3.05	287.3	2.07×10^5	0.277	MST-3
4.35	263.8	2.08×10^5	0.281	MST-4

Eq. (4) is used to illustrate out-of-plane initial distortion shape with combination of amplitude function in plate using Eq. (5). In Eq. (4), initial distortion shape with three- and one-half waves is taken into account in the longitudinal and transverse direction, respectively ($m = 3$ and $n = 1$). Average and severe levels of the initial distortion of the plate member are separately applied to each finite element model. It is assumed that the level of initial distortion corresponds to the level of weld residual stress. For instance, the average level of the residual stress is always paired with the average level of the initial distortion. In case of the stiffener web, out-of-plane deflections are determined by Eq. (6), while in-plane distortions by the second term of right hand side of Eq. (4). Amplitudes of vertical and lateral deflections are assumed to be 0.15% of frame space of 540 mm, as delineated in Eq. (7).

$$\delta_p(x,y) = C_p \sin\frac{m\pi x}{a}\sin\frac{\pi y}{b} + C_s \sin\frac{\pi x}{a} \tag{4}$$

$$\frac{C_p}{t_p} = \begin{cases} 0.025\beta^2 & for\ slight\ level \\ 0.1\beta^2 & for\ average\ level \\ 0.3\beta^2 & for\ severe\ level \end{cases} \tag{5}$$

$$\delta_w(x) = C_w \sin\frac{\pi x}{a} \tag{6}$$

$$C_s = C_w = 0.0015a \tag{7}$$

Unless initial distortion is symmetric with respect to y-plane shown in Fig. 2(a), it is impossible to see exactly symmetric hogging or sagging deformation since neutral axis becomes to rotate due to the asymmetry of the initial distortion. Therefore, only symmetric initial distortion shapes are considered as depicted in Fig. 2(b) and (c) where each represents concave and convex about base plate, respectively. It is assumed that initial distortion at the attachment line between plate and stiffener web is always concave toward the stiffener web (convex toward the plate). This may accelerate local lateral buckling of stiffener web unless initial distortion mode is changed to higher order modes during shortening process.

Many authors have proposed ultimate strengths or moment-carrying capacities using nonlinear FEA where most of them were based on one frame span model, because it is believed that a hull girder usually collapses in the middle of two successive frames at mid-ship. It is generally true in reality, but it should be noted that results based on nonlinear FEA with one frame model are more or less affected by boundary conditions in both longitudinal end planes as delineated in Fig. 3(a). Nishihara (1984) presented the moment versus vertical deflection data at mid-span of the box girder shown in Fig. 1(b), hence long span FE models are also prepared in Fig. 3(b) where lengths of elastic part and elasto-plastic part are 2000 mm and 650 mm in symmetric model, respectively.

In case of the one frame model shown in Fig. 3(a), two reference nodes are located at centroids of the box girder end planes. In order that plane end sections remain plane, dependencies between a reference node and the end plane nodes are required. A reference node on an end is linked to end plane

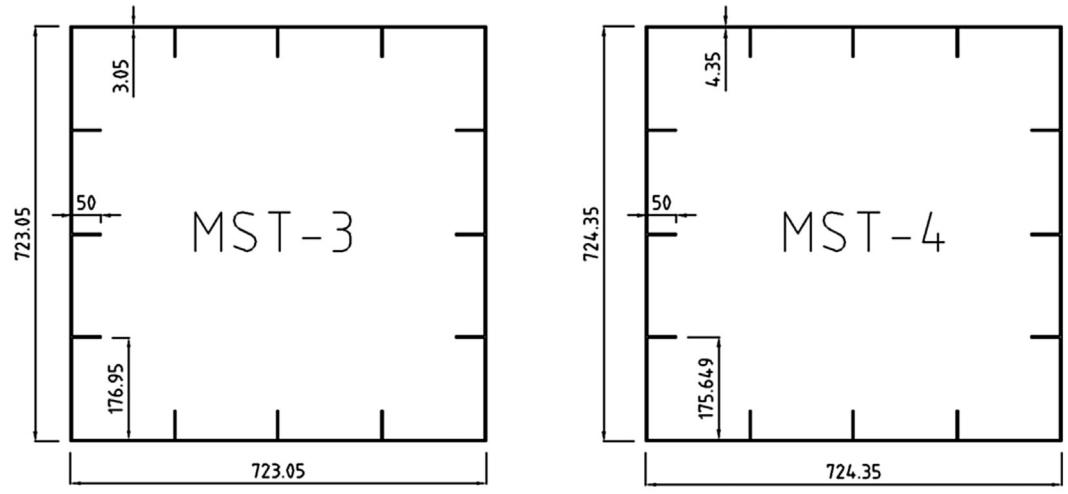

(a) Box girder sections entitled MST

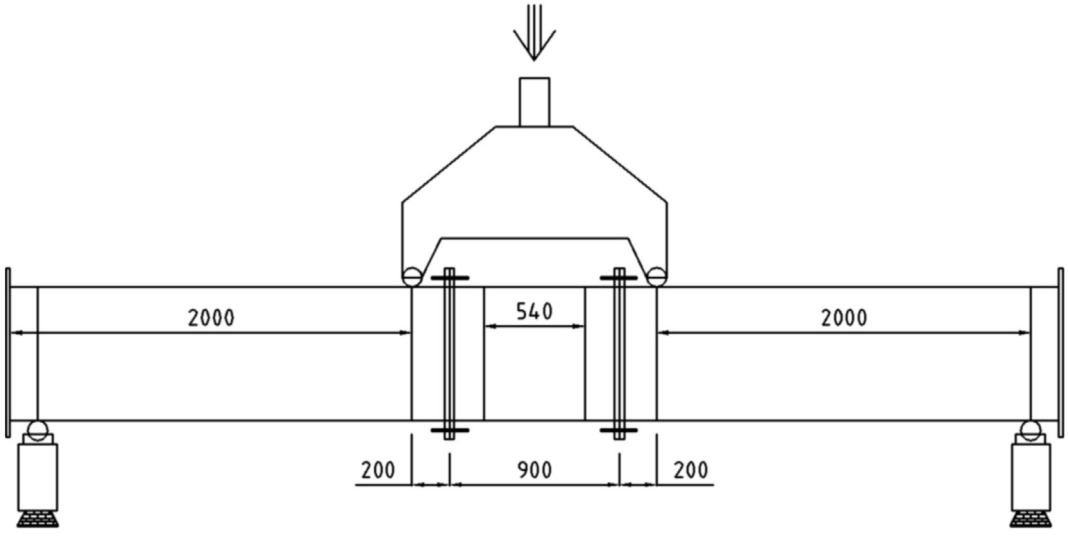

(b) A sketch of collapse test

Fig. 1. Box girder model and test specimen (Nishihara, 1984).

nodes with translational dependency along x- direction and rotational dependencies about x-, y-, and z-directions. Boundary conditions at the reference nodes should be decided so that neutral axis can smoothly shift down along z-direction under sagging moment. Prescribed rotations are applied to two reference nodes. Symmetry boundary conditions are also imposed on the nodes located at mid-plane. All boundary conditions for one frame model are summarized in Table 2.

Simply supported boundary condition is used at the bottom end of long span model shown in Fig. 3(b). Symmetry boundary conditions are also applied to the mid-plane nodes of the long span test model. Prescribed vertical displacement is applied to the hydraulic loading lines (refer to Fig. 1(b)). All boundary conditions for the long span model are summarized in Table 3.

Twelve elements and five elements are arranged for a longitudinal space of plate and a stiffener web height, respectively, including weld-induced tensile yield stress zones. Nominal element sizes for a stiffener spacing and a stiffener are approximately less than 15 mm and 10 mm for most of box girders. Even though a convergence test to seek suitable element sizes has not been carried out in this study, it is thought that the numbers of elements used for plate and stiffener web are sufficient to simulate any global and local buckling modes.

A commercial finite element code Abaqus/Standard is used for all simulations. Adequate number of elements make it possible to use quadrilateral element with reduced integration scheme (S4R) which is capable of deforming to a large strain. One dimensional dummy elements with axial degree of freedom (T3D2) with very small section area (nearly zero) are arranged to capture neutral axis movement. Change of axial stress signs between two successive curvature increments tells location of neutral axis in vertical direction.

Only elastic material properties listed in Table 1 are applied to out of the pure bending part of the long span model in

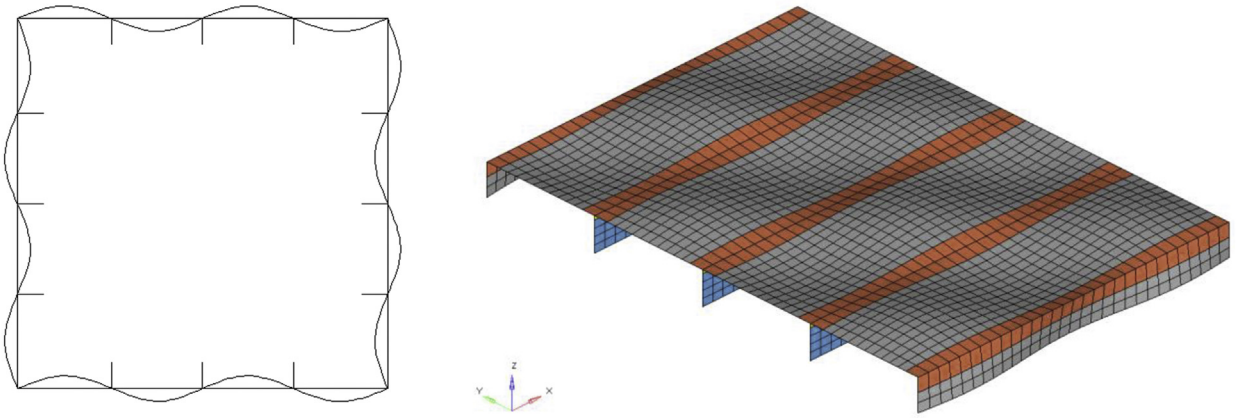

(a) Asymmetric initial distortion

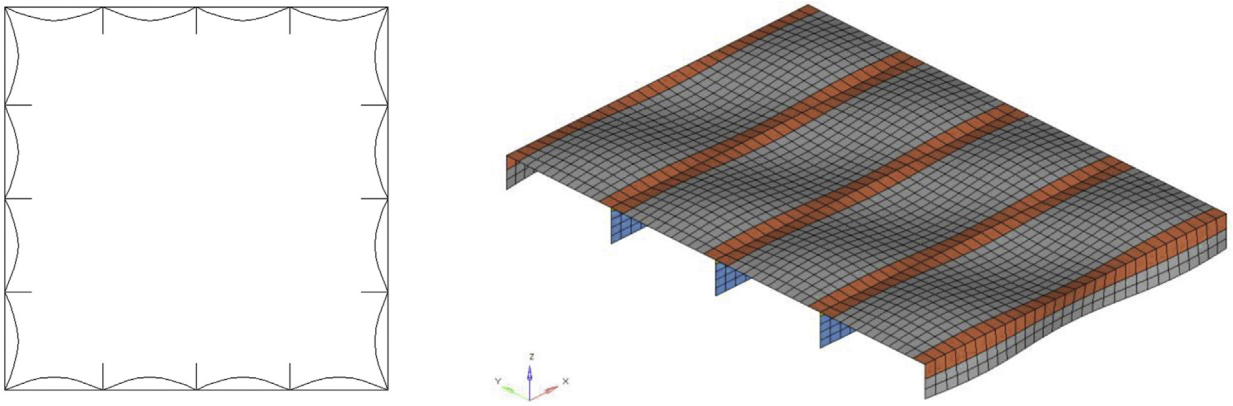

(b) Symmetric initial distortion (concave to plate)

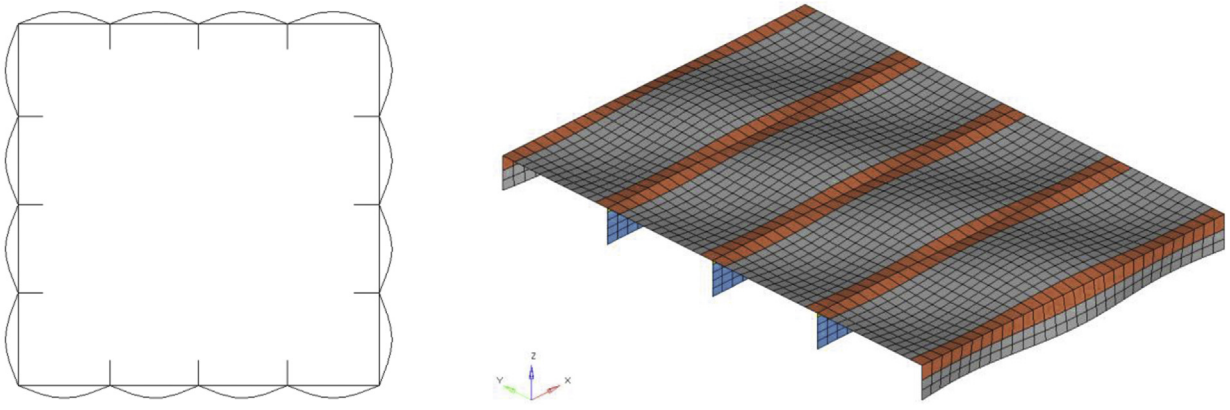

(c) Symmetric initial distortion (convex to plate)

Fig. 2. Scaled initial distortion shapes.

Fig. 3(b). Elastic-perfect plastic material properties listed in Table 1 are assigned to all other parts. The numbers of elements in the one frame model and the long span test model are 13,082 and 54,188, respectively.

Analysis cases are listed in Table 4 which are categorized according to thicknesses of base plates, test types (model extents), levels of initial imperfections, and direction of initial distortion. Sixteen analysis cases are considered in total.

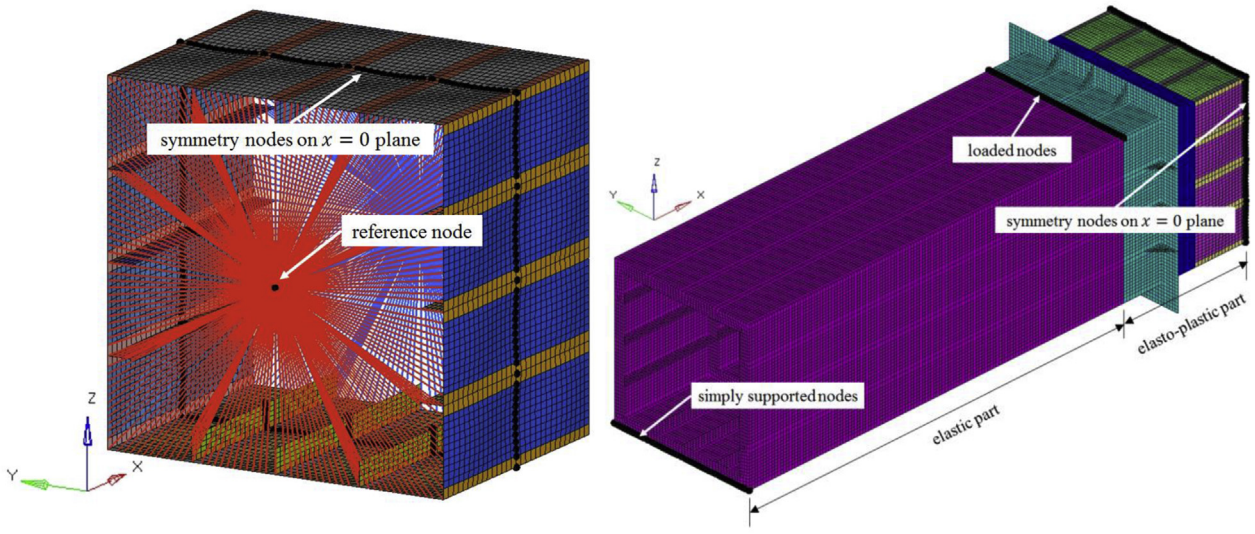

(a) One frame model (b) Long span model

Fig. 3. Finite element analysis models.

Table 2
Applied boundary conditions and load conditions on one frame model.

Boundary conditions	Constraints and load
Reference nodes on end planes	$R_x = R_z = 0$ and prescribed R_y inducing sagging deformation
Symmetry nodes on mid-plane	$T_x = R_y = R_z = 0$

Table 3
Applied boundary conditions and load conditions on long span model.

Boundary conditions	Constraints and load
Symmetry nodes on mid-plane	$T_x = R_y = R_z = 0$
Simply supported nodes	$T_y = T_z = R_x = 0$
Loaded nodes	Prescribed T_z inducing sagging deformation

2.3. Moment-carrying capacities

Fig. 4(a) and (b) represent comparisons of moment carrying-capacities for the test cases of MST-3 and MST-4, respectively. As previously discussed, level of initial imperfection significantly affects moment-carrying capacity of the box girder and effect of initial imperfections is well reflected in elastic slope shown in Fig. 4. It means that elastic stiffness difference of MST-3 due to initial imperfections is much more remarkable than that of MST-4. This is why welding distortion in thin plate usually reaches higher levels.

In both test cases of MST-3 and MST-4, ultimate strengths from nonlinear FEA simulations for the one frame models with average level of initial imperfection appears to be in upper bound compared to the test results. Considering relatively thicker plates are used in real ship structures, hence it is inferred that weld-induced initial distortions would be developed in the box girder specimens. More accurate prediction of ultimate strength from the one frame model is seen when the severe level of initial imperfections is assumed.

Fig. 5 shows comparison of moment-carrying capacities for the test cases of MST-3 and MST-4. The ultimate strength obtained from the MST-3 experiments agrees well with the simulation cases of MST3-LSM-SEV-CV and MST3-TM-SEV-CX in which severe level of initial imperfection is assumed. Meanwhile, ultimate strength from the MST-4 test seems to lies in the middle of those corresponding to results from FEA models with average and severe levels of imperfections. As the authors pointed out in Fig. 4, because initial imperfection level tends to be reduced as thickness of the plating increases, these tendencies can be explained using correlation between plating thickness and initial imperfection level.

There might be a lucid explanation why the vertical displacement from nonlinear FEA does not coincide with the test one. Geometry details of the elastic part which was used to produce pure bending moment between two hydraulic loading points in Fig. 1(b) were not presented in Nishihara (1984). The only data was thickness of 6 mm in the elastic part. It is assumed that Nishihara (1984) might use same size stiffeners and frame spacings of the elastic part fabrication as the middle part. Not only the vertical deflections in the box girder collapse tests might include any clearances between bottom supports and load frame, but also scheme for bolt-fastening was not described in the original article. In MST-3 and MST-4, it can be concluded that the one frame and long span models well predict maximum moment capacities as long as suitable level of initial imperfection are secured.

3. A new procedure to extract LSE curves (step II)

3.1. Discretization into structural units

PCM is simple to use and known to provide relatively accurate results, but it is largely dependent on accuracy of

Table 4
Summary of nonlinear FEA cases.

Model label	Base plate		Model extent		Level of initial imperfection		Direction of initial distortion	
	MST-3	MST-4	One frame model	Long span model	Moderate	Severe	Concave	Convex
MST3-OFM-MOD-CV	V		V		V		V	
MST3-OFM-MOD-CX	V		V		V			V
MST3-OFM-SEV-CV	V		V			V	V	
MST3-OFM-SEV-CX	V		V			V		V
MST3-LSM-MOD-CV	V			V	V		V	
MST3-LSM-MOD-CX	V			V	V			V
MST3-LSM-SEV-CV	V			V		V	V	
MST3-LSM-SEV-CX	V			V		V		V
MST4-OFM-MOD-CV		V	V		V		V	
MST4-OFM-MOD-CX		V	V		V			V
MST4-OFM-SEV-CV		V	V			V	V	
MST4-OFM-SEV-CX		V	V			V		V
MST4-LSM-MOD-CV		V		V	V		V	
MST4-LSM-MOD-CX		V		V	V			V
MST4-LSM-SEV-CV		V		V		V	V	
MST4-LSM-SEV-CX		V		V		V		V

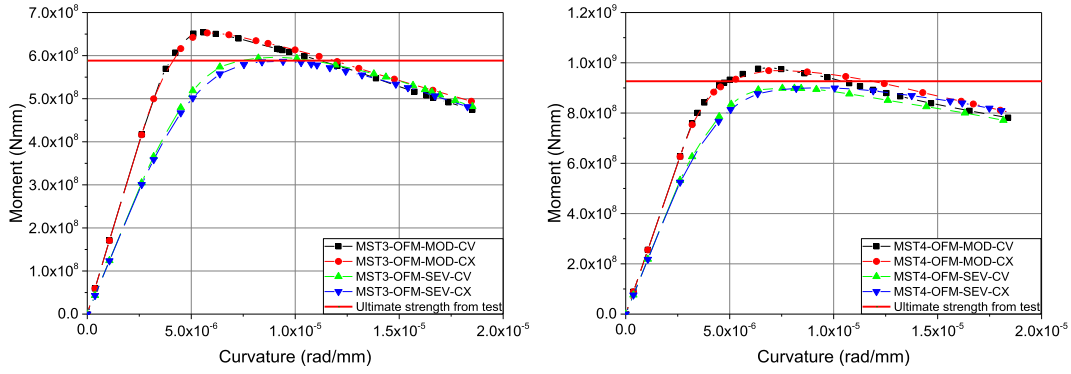

(a) MST-3 (b) MST-4

Fig. 4. Comparison of moment versus curvature diagrams from one frame-based nonlinear FEAs and actual tests.

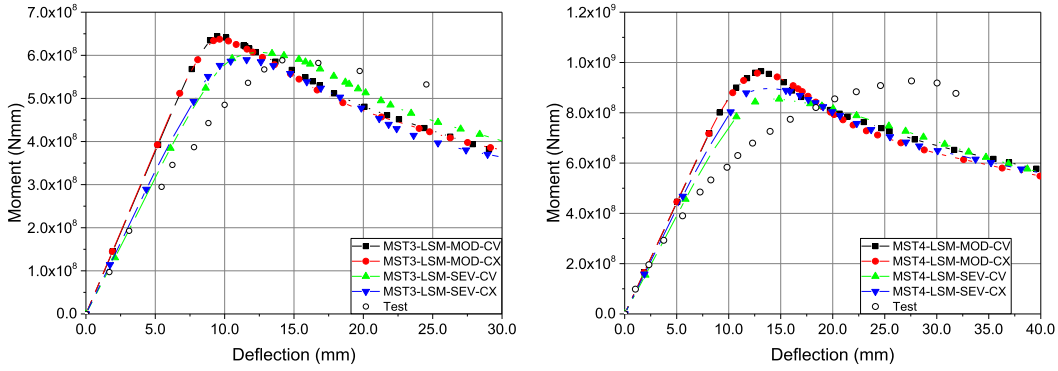

(a) MST-3 (b) MST-4

Fig. 5. Comparison of moment versus curvature diagrams from long span box girder FEAs and actual tests.

LSE curves of structural units. For this reason, many approaches have been proposed to build accurate LSE data. After Common Structural Rules (CSR) came into effect in 2006 (IACS, 2015), CSR-based simplified formulas have been dominantly used to assess hull girder ultimate strengths because the rules including the formulas have been imbedded in many softwares developed by classification societies.

In Section 2, reliability of nonlinear FEA is discussed by comparing FEA-based moment carrying-capacities with test ones whether FEA model is one framed or long spanned. Since the fundamental aim of this study is to verify how accurate PCM can estimate moment-carrying capacities, so a new procedure to construct LSE data is to be introduced in Section 3.

For the problem to be simple, only the one frame model delineated in Fig. 3(a) is taken into account hereafter to extract LSE curves. The first job to extract LSE curves is to discretize the box girder section to a sufficient number of structural units. The objective box girders are composed of only three stiffened panels in deck, side, or bottom, respectively, hence finer size structural units are needed than the current size stiffened panels. Otherwise moment-curvature relation and neutral axis shift will be discontinuous since there are only three stiffened panels in box girder sides. In this study, 44 structural units are used as shown in Fig. 6(a). As Fig. 6(b) represents nodes in nonlinear FEA, a LSE curve of a structural unit can be produced using approximately five finite shell elements.

If this box girder is under sagging deformation, the structural units at deck level will experience the severest axial shortening loads, while the structural units located above neutral axis are to be under compression. Therefore load-shortening data from the deck level structural units can be resistance curves under compressive loads, while load-elongation data from the structural units on bottom can be resistance ones under tension loads.

Axial shortening or elongation force ($f_{x,i}$) of ith finite element can be taken from nonlinear FEA results. In other words, a compressive or tensile section force which is integral of axial stress ($\sigma_{x,i}$) with respect to thickness (t) can be taken from FEA results. Then multiplication of the section force by width of the finite element (b_i) yields axial force of the finite element as depicted in Eq. (8). Summation of the axial forces from the finite elements which are belonged to a structural unit becomes LSE data for the structural unit.

$$f_{x,i} = b_i \int_{-\frac{t}{2}}^{\frac{t}{2}} \sigma_{x,i} dz \tag{8}$$

3.2. Analyses of LSE data

For sagging moment-induced symmetry deformation, the load-shortening capacity of the structural unit #23 should be same as that of the structural unit #33. In addition, the load-shortening curve of the structural units #23 under sagging condition can be used for the other corner structural units of #1 and #11 under hogging condition. Similarly, LSE behaviors are considered to be same for the structural units of #2, #10, #24, and #32. The other units can be easily grouped according to dimensions and locations of structural units.

After applying sagging moment to the one frame box girders, the load-shortening curves for the structural units #23–#28 and the load-elongation curves for the structural units #6–#11 are collected in Fig. 7. Observation on third quadrants (load-shortening zones) of Fig. 7 reveals that assumption of convex initial deformation induces early collapse of two longitudinal webs (units #25 and #28). It may be because lateral torsional buckling occurs in the mid-span of the box girder (refer to Fig. 7(b)). Existence of initial deformation in bottom area under sagging moment helps to reduce initial distortion like a stretching of crumpled papers. This is why inelastic strain ($\varepsilon/\varepsilon_{y0}$) starts after unity value. The increased starts of inelastic strains are well addressed in Fig. 7(c), (d), (g), and (h) with severe level of initial distortion.

Sometimes, it is observed that LSE data slightly exceed unity value. Cross section area of a stiffener web in FEA

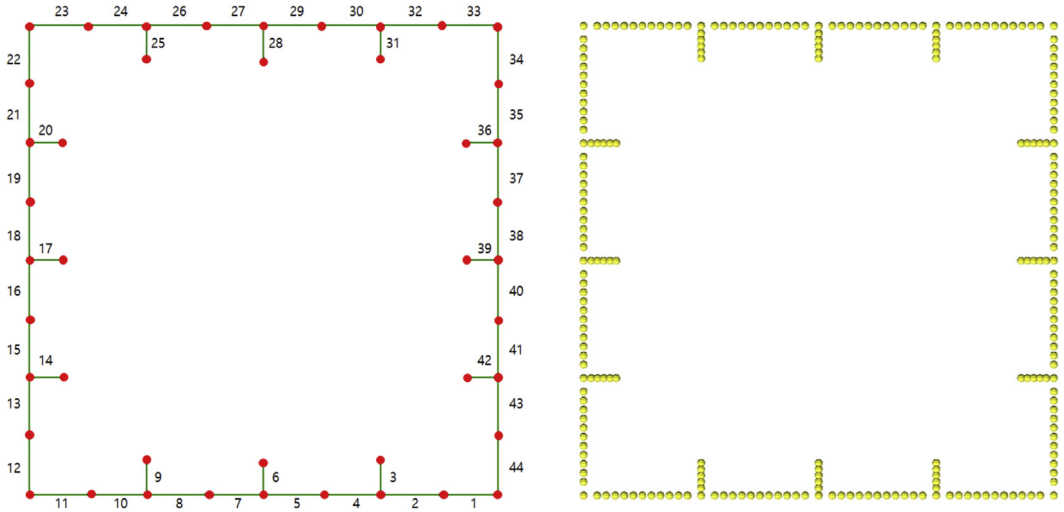

(a) Structural units for PCM (b) Nodes for nonlinear FEA

Fig. 6. Comparison of hull section discretization.

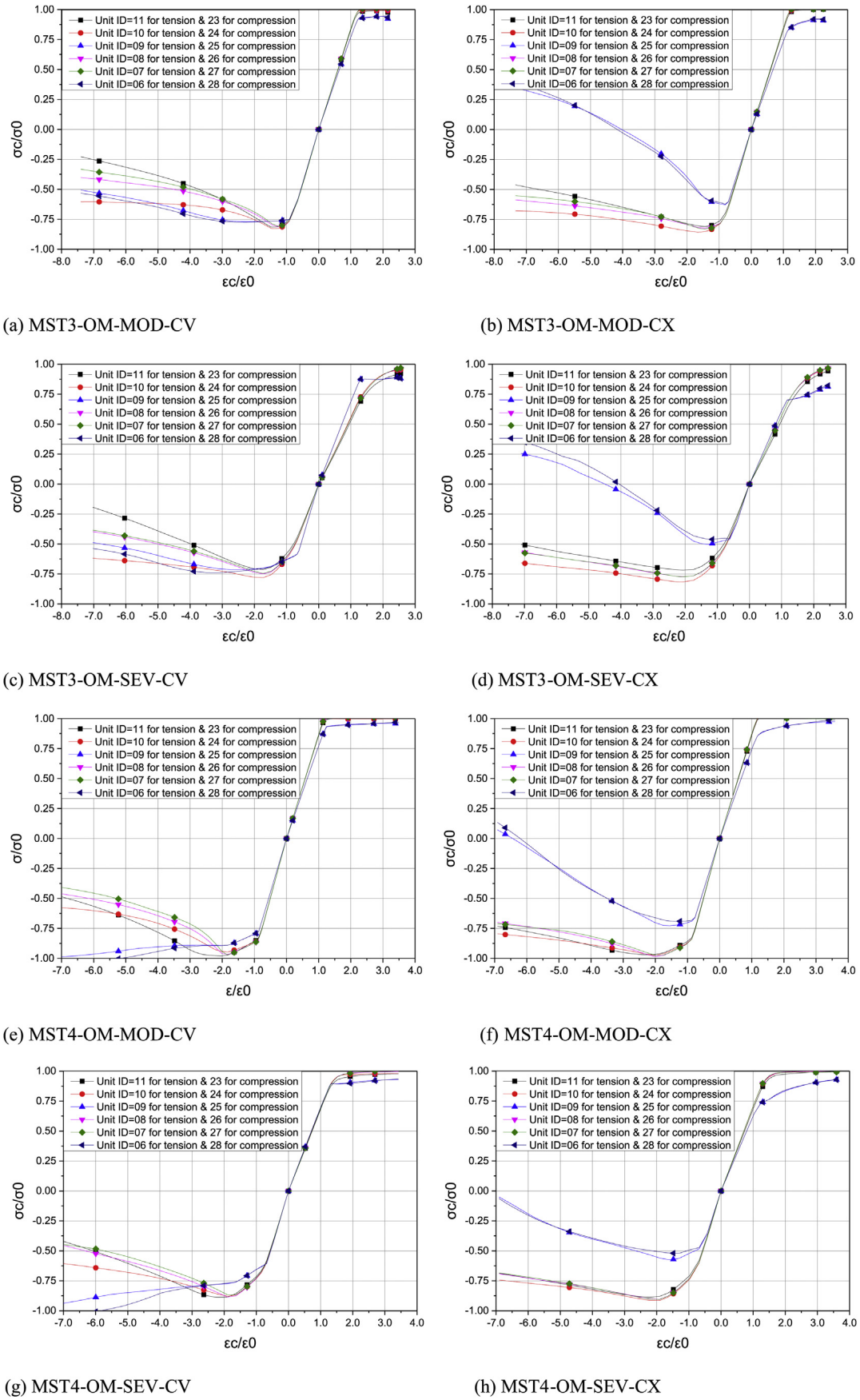

Fig. 7. LSE curves extracted from the box girder nonlinear FEAs.

model is slightly larger than actual area because the stiffener web height is measured from mid-thickness of plate. But they are considered to be within the numerical tolerance ranges.

Unit #23 should be considered as a hard corner unit in common structural rules (IACS, 2015). Remembering that a hard corner unit is assumed to behave elastic-perfect plastic, it should be noted that any elastic-perfect plastic load-shortening behavior is not observed in unit #23. It means if more accurate LSE data we have, there might be no need to use a hard corner unit which will lead to more precise ultimate strength calculation.

4. Comparison of moment-carrying capacities of the box girders (step III)

4.1. Application of LSE data into PCM

In-house code UMADS which has been developed to predict moment-carrying capacity of an intact and asymmetrically damaged hull section is used to realize PCM (Choung et al., 2014). UMADS is capable of importing LSE curves which are externally generated. A ship section is conveniently constructed and visualized in UMADS where properties of the imported LSE data can be reviewed. Finally, execution of UMADS carries out calculation of moment-carrying capacity simulating translational and rotational shifts of neutral axis (refer to Fig. 8).

4.2. Comparison of moment-carrying capacities of the box girders

As described in Fig. 8, LSE data listed in Fig. 7 are used as input of UMADS. Fig. 9 shows comparison of moment-carrying capacities obtained from nonlinear FEA and PCM. In some cases shown in Fig. 9(a), (c), (e), (g), and (h), it is certain that PCM-based moment carrying-capacities are perfectly coincided with nonlinear FEA-based ones until each curvature reaches pre-assigned termination value. Difference in neutral axis histories is in an increasing trend in cases depicted in Fig. 9(b), (d), and (f), but moment versus curvature relations are still good agreement between results from FEA and PCM. This says that neutral axis shift history is very important for accurate prediction of moment-carrying capacity. From Fig. 9, it can be concluded that PCM is almost equivalent to nonlinear FEA as long as accurate LSE curves are secured and consequently neutral axis mobility is well predicted.

5. Discussion: application of the new procedure to real ship hull sections

It is inevitable to encounter significant obstacles to apply the new procedure introduced in this paper to real mid-ship

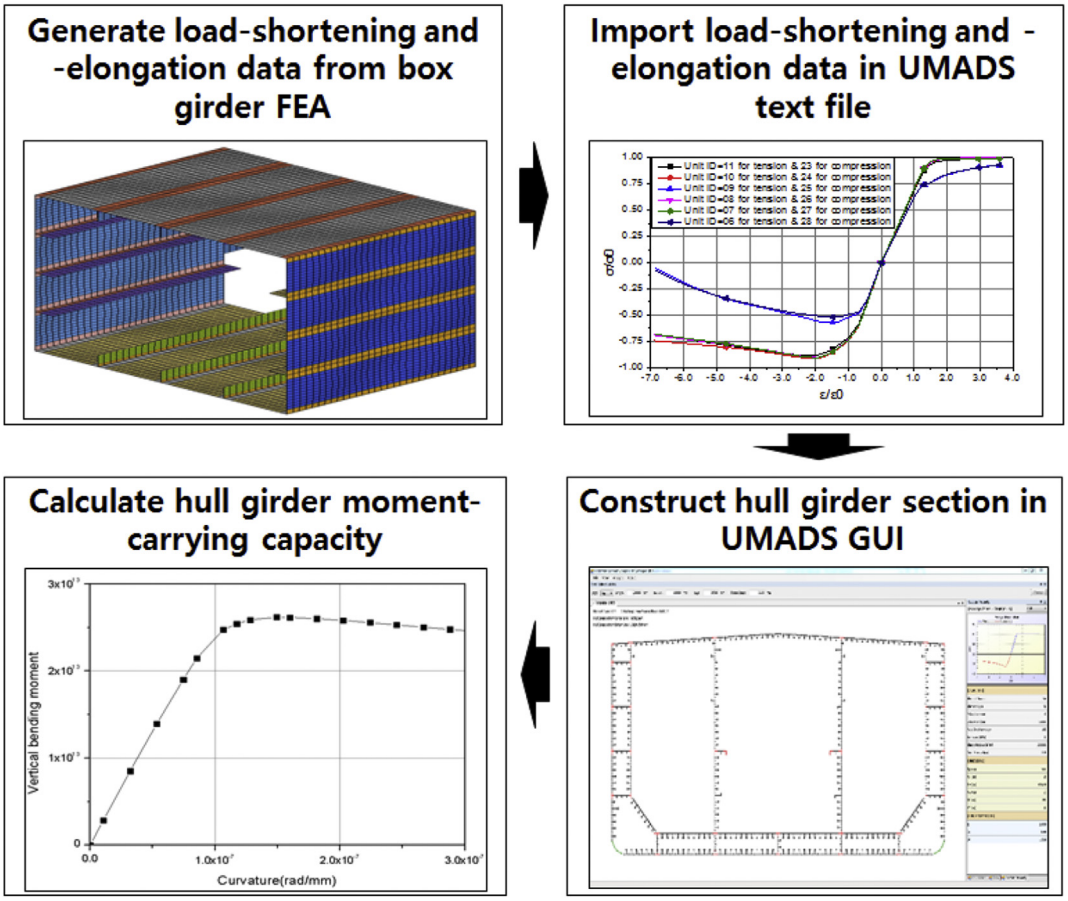

Fig. 8. Derivation of moment-carrying capacity using box girder FEA and UMADS.

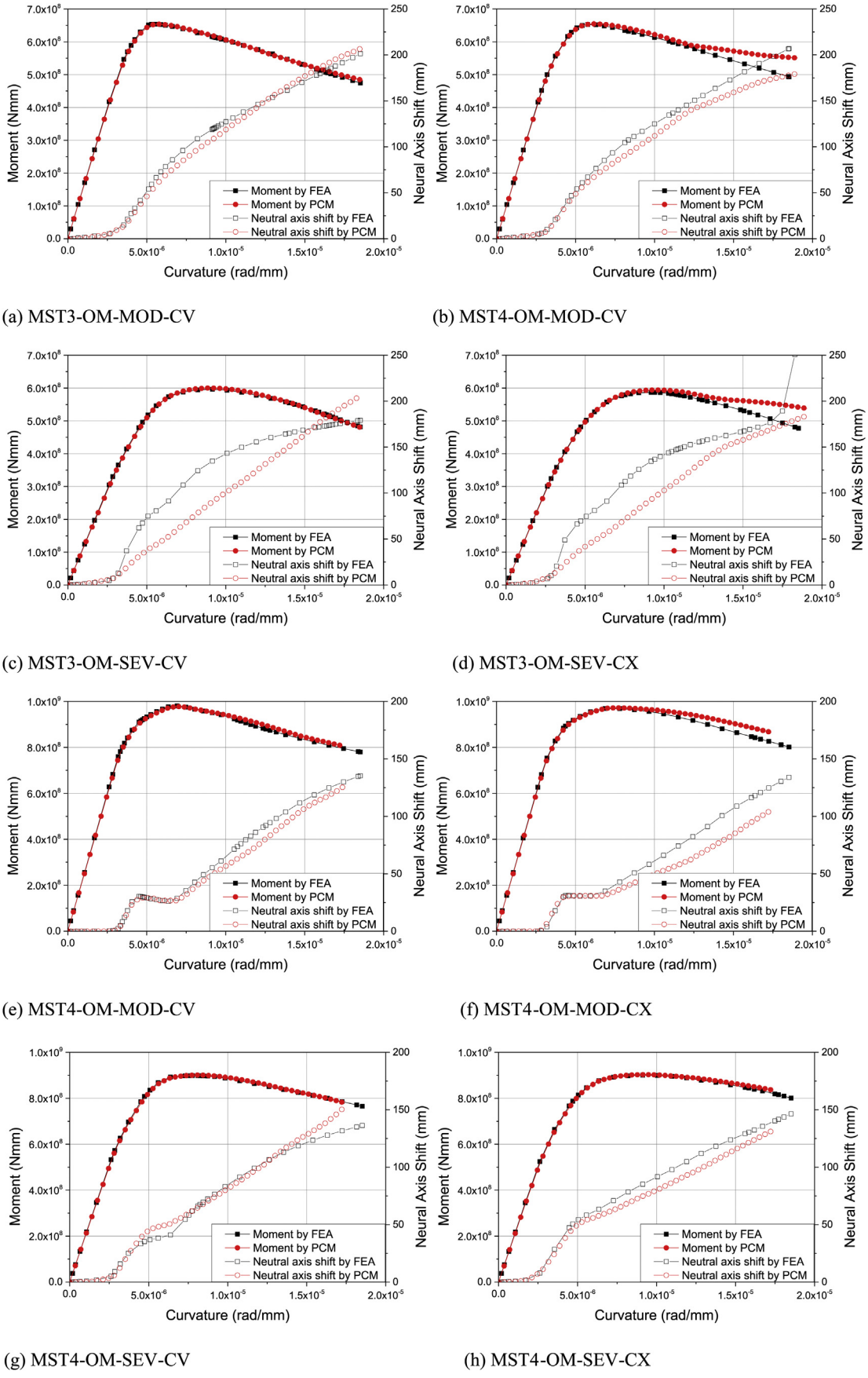

(a) MST3-OM-MOD-CV (b) MST4-OM-MOD-CV

(c) MST3-OM-SEV-CV (d) MST3-OM-SEV-CX

(e) MST4-OM-MOD-CV (f) MST4-OM-MOD-CX

(g) MST4-OM-SEV-CV (h) MST4-OM-SEV-CX

Fig. 9. Comparison of moment-curvature curves and neutral axis shift-curvature curves.

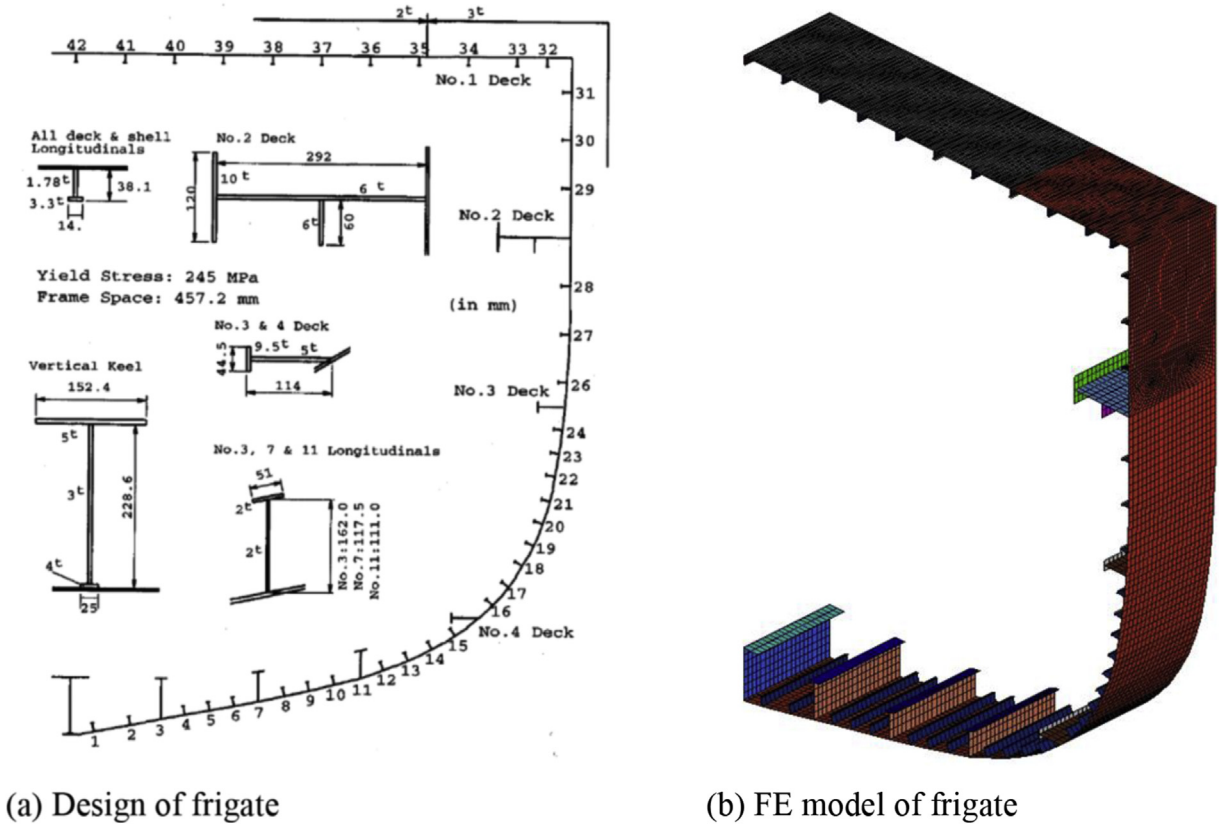

Fig. 10. FE model of 1/3 scale frigate.

section. The most significant problem is that a large number of box girder models are required to obtain the load-shortening and -elongation data for a real ship section. Next problem for application of the new procedure is that transverse location of a stiffener should be taken into account. This is mainly due to shear lag effect and severity of buckling deformation, thus two LSE data taken from two structural units with same dimensions may not be same if two are in different transverse locations.

Well-known 1/3 scale frigate model (ISSC, 2000) is chosen to see how many box girder models are required to obtain LSE data (refer to Fig. 10(a)). A FE model for the frigate is also prepared with average level of initial distortion as shown in Fig. 10(b) to which same boundary conditions presented in Table 2 are applied.

Even for 1/3 scale frigate model depicted in Fig. 10 which is thought to be not so much complicated hull section, at least 20 box girder models are required considering dimensions in stiffeners attached to plate and transverse locations. For example, stiffener #34 in Fig. 10(a) has same dimensions of the stiffener with #42–#36, but thicker plate thickness and shorten width force to produce additional box girder model. A summary to determine the number of box girder models is shown in Table 5.

Stiffened panels of #36–#42 and #16–#24 which are located on deck plate and side shell, respectively, are selected for in-depth discussion on load shortening behaviors. A sagging and a hogging moments are applied to the frigate model to take out load shortening data for the stiffened panels of #36–#42 and #16–#24, respectively.

Then two box girder models representing deck plate stiffened panels of #36–#42 and side shell stiffened panels of #16–#24 are generated as shown in Fig. 11(a) and (b), respectively. Two are names as BG-S (box girder for side shell stiffened panels) and BG-D (box girder for deck plate stiffened panels). Stiffener spacing in side shell stiffened panels of #16–#24 is narrower than that in deck plate stiffened panels of #36–#42, so many stiffeners are arranged for BS-S. Stiffened panels in BG-S are labeled like S-01, S-02, S-03 … S-20, while stiffened panels in BG-D like D-01, D-02, D-03 … D-10.

Fig. 11(a) and (b) also present post-ultimate deformed geometries where very uniform deformation shapes are found for BG-D, while non-uniform buckling deformation shapes in BG-S. It means that almost unified LSE data are expected for stiffened panels located at deck or bottom of BG-D. However significant scatter in LSE data for stiffened panels located at deck or bottom of BG-S is expected.

Load-shortening data from two box girders of BG-S and BG-D are shown in Fig. 12(a) and (b). Load-shortening data for BG-D looks single curve because they are almost perfectly coincident. But load-shortening data for BG-S show serious deviation after maximum shortening load. Narrower stiffener spacing and reduced scantling of stiffener may lead to local buckling mode in stiffened panels in BG-S. In this case, we have one more uncertainty to choose LSE data, because it is impossible to predict occurrence and degree of development of

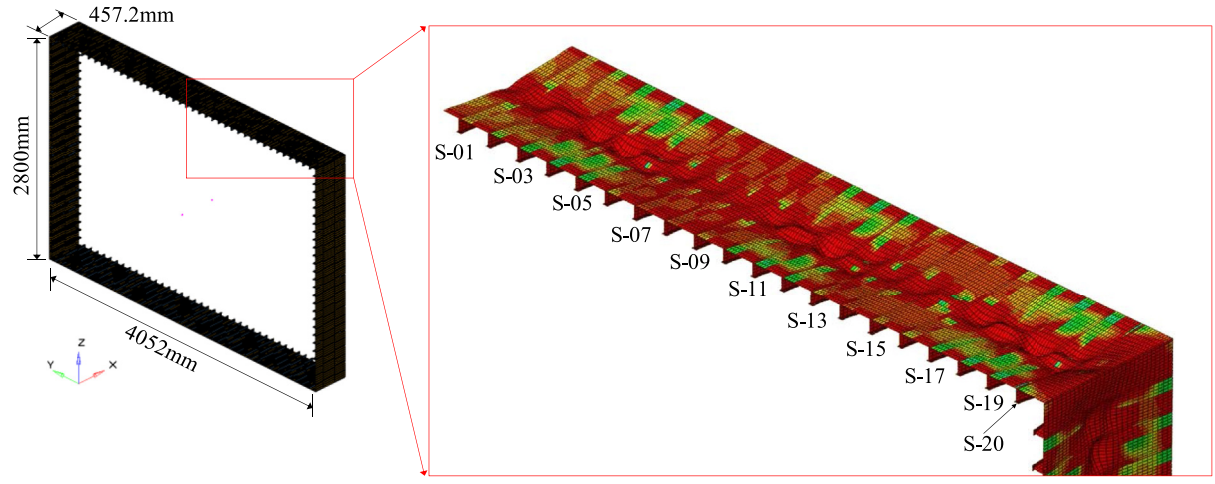

(a) BG-S representing side shell stiffened panels of #16-#24

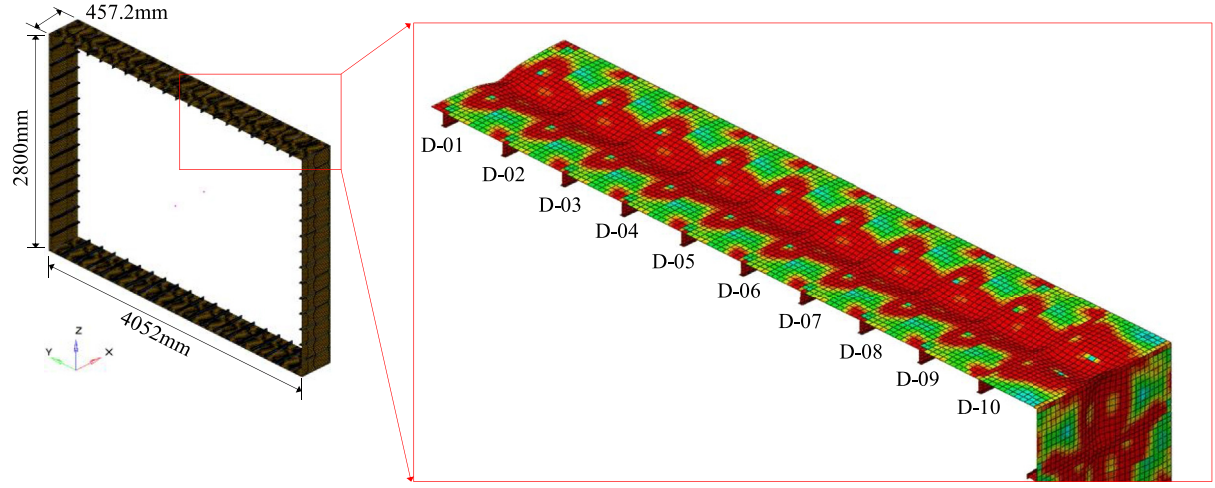

(b) BG-D representing deck plate stiffened panels of #36-#42

Fig. 11. Hull section and box girder model for 1/3 scale frigate.

Table 5
A table for prediction of the number of box girder models necessary for the 1/3 scale Frigate (mm).

Box girder model no.	Stiffener no.	Plate thickness	Plate width	Stiffener size	Remarks
1	Vertical keel	3.0	50.00	228.60 × 3.40 + 152.45 × 5.00	Equivalent web thickness
2	1–2	3.0	140.40	38.1 × 14.0 × 1.78/3.3	
3	3	3.0	113.80	162.0 × 2.0 + 51.0 × 2.0	Stiffener web assumed to be perpendicular to side shell
4	4–6	3.0	102.40	38.1 × 14.0 × 1.78/3.3	
5	7	3.0	105.40	117.5 × 2.0 + 51.0 × 2.0	Stiffener web assumed to be perpendicular to side shell
6	8–10	3.0	107.70	38.1 × 14.0 × 1.78/3.3	
7	11	3.0	106.40	111.0 × 2.0 + 51.0 × 2.0	Stiffener web assumed to be perpendicular to side shell
8	12–15	3.0	110.00	38.1 × 14.0 × 1.78/3.3	
9	No 3–4 deck	3.0	100.00	114.0 × 44.5 × 5.0/9.5	
10	16–24	3.0	100.00	38.1 × 14.0 × 1.78/3.3	
11	26	3.0	150.00	38.1 × 14.0 × 1.78/3.3	
12	27–30	3.0	200.00	38.1 × 14.0 × 1.78/3.3	
13	31	3.0	175.00	38.1 × 14.0 × 1.78/3.3	
14	No 2 deck	3.0	200.00	292 × 7.23 + 120 × 10	Equivalent web thickness
15	Hard corner	3.0	56.60	56.6 × 3.0	One side
16	32	3.0	113.15	38.1 × 14.0 × 1.78/3.3	
17	33	3.0	157.90	38.1 × 14.0 × 1.78/3.3	Averaged plate width
18	34	3.0	202.60	38.1 × 14.0 × 1.78/3.3	
19	35	2.5	202.60	38.1 × 14.0 × 1.78/3.3	
20	36–42	2.0	202.60	38.1 × 14.0 × 1.78/3.3	

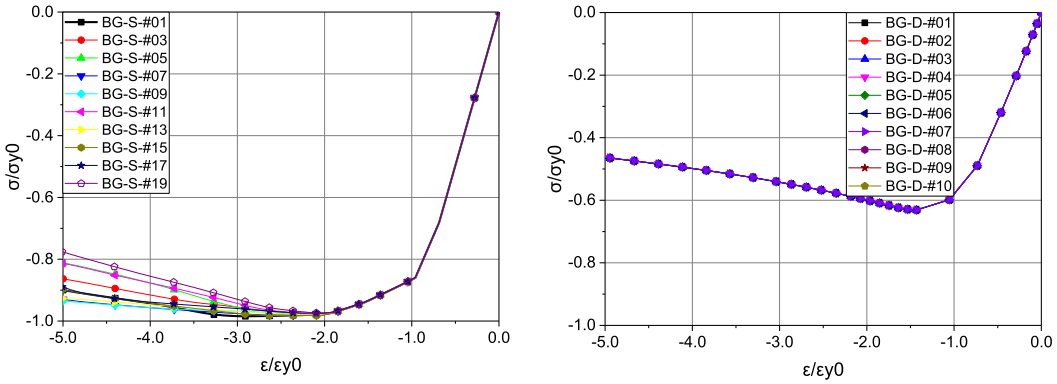

(a) BG-S representing side shell stiffened panels of #16-#24

(b) BG-D representing deck plate stiffened panels of #36-#42

Fig. 12. Load-shortening curves obtained from two box girders.

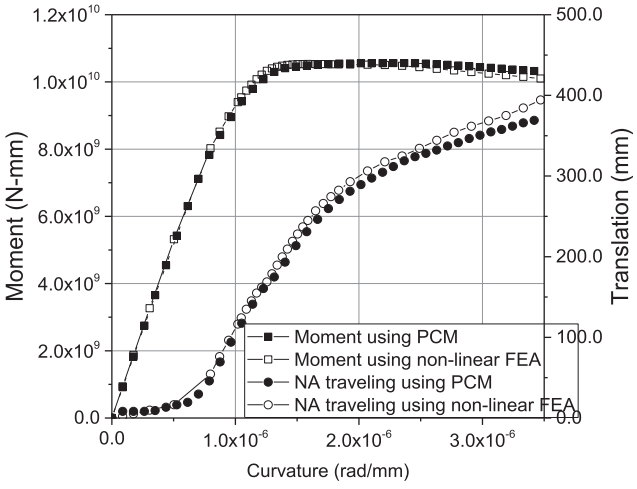

Fig. 13. Comparison of moment-curvature curves and neutral axis shift-curvature curves for 1/3 scale frigate model.

local buckling deformation in stiffened panels in a real ship section. Reminding primary aim of this paper is to introduce feasibility of a new approach to estimate more reliable LSE data based on box girder FE models, a load-shortening data corresponding to #01 stiffened panel in BG-S(BG-S-#09 in Fig. 12(a)) is chosen for stiffened panels of stiffened panels of #36–#42 in the frigate.

Fig. 13 shows comparison of moment-carrying capacities between non-linear FEA and PCM with box girder-based shortening data where very excellent coincidence for two curves is found. In addition, neutral axis histories are well coincided each other.

6. Conclusions

PCM which has been popularly used for estimation of hull girder ultimate strength or moment-carrying capacity, but reliability of PCM is known to be largely dependent on accuracy of LSE data. The substantial aim of this paper is to introduce the new procedure to obtain LSE data from nonlinear FEAs of box girder models, thus the new approach is expected to contribute to accuracy improvement of PCM-based hull girder ultimate strength.

Prior to discussing the new approach, in order to minimize other probable uncertainties in numerical simulations relative to experimental results, it is decided to select the simple box girders tested by Nishihara (1984) instead of selecting complicated of hull girder. Nonlinear FEAs-based moment-carrying capacities of the simple box girders are studied for verification with test results. Consequently, reliability of the applied nonlinear FEAs has been proved to be effective.

It has been explained that LSE datum for a structural unit is summation of axial stresses for a couple of elements comprising the structural unit. An axial stress is conveniently obtained by integrating section forces about each element thickness. The box girder is discretized into 44 structural units for which LSE data are obtained from the box girder FEA. Inserting the LSE data corresponding 44 structural units to UMADS, box girder moment-carrying capacity is compared with box girder FEA results. Much outstanding coincidences are found for box girder models with different initial imperfection modes and amplitudes.

Practical example of application of the new procedure is introduced in discussion section. The 1/3 scale frigate model is selected for application study. It is found that 20 box girders are required to obtain LSE data for the frigate model. Buckling mode and amplitude are found to be very important factors determining post-ultimate behaviors of LSE data. As long as buckling deformation keeps uniform column mode, almost identical LSE data are generated. If local buckling exists, post-buckling strengths are significantly different according to spatial locations of stiffened panels. An in-house code UMADS based on PCM is used to generate moment-carrying capacity with LSE data from the box girder models. It is proved that two approaches of PCM and nonlinear FEA are almost equivalent in terms of moment-carrying capacity and neutral axis shift as long as accurate LSE curves are secured.

It should be noted that in order to apply the newly proposed procedure to a real ship section composed of dozens of

stiffened panels, a large number of non-linear box girder FEAs is required. Hence, development of box girder modeling tool which should be capable of taking into account weld-residual stress effect and initial distortion is urgent in near future. In case that post-buckling strengths of same sized stiffened panels are quite different, how we can select suitable LSE data is future challenge. In addition, applicability of extended box girder model to minimize boundary effect, for example three framed box girder model, should be studied for future work. LSE data of various types of hard corner units have to be assessed quantitatively.

Acknowledgment

This research (work) was financially supported by the 1) "Korea-UK Global Engineer Education Program for Offshore Plant" funded by the Ministry of Trade, Industry & Energy (MOTIE), Korea and 2) "Manpower training program for ocean energy" funded by the Ministry of Oceans and Fisheries (MOF), Korea.

References

Amlashi, H.K.K., Moan, T., 2008. Ultimate strength analysis of a bulk carrier hull girder under alternate hold loading condition – a case study Part 1: nonlinear finite element modelling and ultimate hull girder capacity. Mar. Struct. 21 (4), 327–352.

Benson, S., Downes, J., Dow, R.S., 2013. Compartment level progressive collapse analysis of lightweight ship structures. Mar. Struct. 31, 44–62.

Caldwell, J.B., 1965. Ultimate longitudinal strength. Trans. RINA 107, 411–430.

Choung, J., Nam, J.M., Ha, T.B., 2012. Assessment of residual ultimate strength of an asymmetrically damaged tanker considering rotational and translational shifts of neutral axis plane. Mar. Struct. 25, 71–84.

Choung, J., Nam, J.M., Tayyar, G.T., 2014. Residual ultimate strength of a very large crude carrier considering probabilistic damage extents. Int. J. Nav. Archit. Ocean Eng. 6, 14–26.

Dow R.S. Testing and analysis of a 1/3-scale welded steel frigate model, In: Proceedings of the International Conference on Advances in Marine Structures, May 21–24, 1991, Dunfermline, Scotland, UK, 749–773.

Gordo, J.M., Guedes Soares, C., 1996. Approximate method to evaluate the hull girder collapse strength. Mar. Struct. 9, 449–470.

Gordo, J.M., Guedes Soares, C., 1997. Interaction equation for the collapse of tankers and container ships under combined bending moments. J. Ship Res. 41 (3), 230–240.

Gordo, J.M., Guedes Soares, C., Faulkner, D., 1996. Approximate assessment of the ultimate longitudinal strength of the hull girder. J Ship Res. 4 (1), 60–69.

Hughes, O.F., Paik, J.K., 2010. Ship Structural Analysis and Design. Society of Naval Architects and Marine Engineers, New Jersey, USA.

International Association of Classification Societies (IACS), 2015. Common Structural Rules for Bulk Carriers and Oil Tankers. IACS.

International Ship and Offshore Structures Congress(ISSC), 2000. Special Task Committee VI.2 Ultimate Hull Girder Strength. 14th ISSC, Nagasaki, Japan, 2000.

Nippon Kaiji Kyokai(NKK), 2014. Investigation Report on Structural Safety of Large Container Ships. NKK.

Nishihara, S., 1984. Ultimate longitudinal strength of mid-ship cross section. Nav. Archit. Ocean Eng. 22, 200–214.

Nam, J.M., Choung, J., Park, S.Y., Yoon, S.W., 2014. Assessment of residual ultimate strength of vlcc according to damage extents and average compressive strength of stiffened panel. In: Proceedings of the ASME 2014 33rd International Conference on Ocean, Offshore and Arctic Engineering (OMAE2014), June 8–13, 2014, San Francisco, California, USA.

Paik, J.K., Kim, D.K., Park, D.H., Kim, H.B., Mansour, A.E., Caldwell, J.B., 2013. Modified Paik-Mansour formula for ultimate strength calculations of ship hulls. Ships Offshore Struct. 8 (3–4), 246–260.

Paik, J.K., Mansour, A.E., 1995. A simple formulation for predicting the ultimate strength of ships. J. Mar. Sci. Technol. 1 (1), 52–62.

Paik, J.K., Kim, B.J., Seo, J.K., 2008. Methods for ultimate limit state assessment of ships and ship-shaped offshore structures: part III hull girders. Ocean Eng. 35, 281–286.

Paik, J.K., Thayamballi, A.K., Che, J.S., 1996. Ultimate strength of ship hulls under combined vertical bending, horizontal bending and shearing forces. Trans. SNAME 104, 31–59.

Qi, E., Cui, W., Wan, Z., 2005. Comparative study of ultimate hull girder strength of large double hull tankers. Mar. Struct. 18, 227–249.

Smith, C.S., 1977. Influence of local compression failure on ultimate longitudinal strength of a ship hull. In: Proceeding of International Symposium on Practical Design in Shipbuilding (PRADS). Tokyo Japan, pp. 73–79.

Smith, C.S., Davidson, P.C., Chapman, J.C., Dowling, P.J., 1988. Strength and stiffness of ships' plating under in-plane compression and tension. Trans. RINA 130, 277–296.

Tayyar, G.T., Nam, J.M., Choung, J., 2014. Prediction of hull girder moment-carrying capacity using kinematic displacement theory. Mar. Struct. 39, 157–173.

Wang, G., Chen, Y., Zhang, H., Shin, Y., 2002. Longitudinal strength of ships with accidental damages. Mar. Struct. 15, 119–138.

Xu, M., Garbatov, Y., Guedes Soares, C., 2013. Ultimate strength assessment of a tanker hull based on experimentally developed master curves. J. Mar. Sci. Appl. 12, 127–139.